Dissipation and transport dynamics in a ratchet coupled to a discrete bath

Jane Rosa and Marcus W. Beims
Departamento de Física, Universidade Federal do Paraná, 81531-990 Curitiba, PR, Brazil
(Received 17 March 2008; revised manuscript received 19 August 2008; published 19 September 2008)

We investigate a particle in a ratchet potential (the system) coupled to an harmonic bath of $N=1-500$ degrees of freedom (the discrete bath). The dynamics of the energy exchange between the system and the discrete bath is studied in the transition regime from low to high values of N. First manifestation of dissipation (energy lost by the system) appears for the bath composed of $10\lesssim N\lesssim 20$ oscillators, as expected. For low values of N, beside small dissipation effects, the system experiences the bath-induced particle transfer between different potential wells from the ratchet. We show that this effect decreases the mobility of particles along the ratchet. The hopping probability along the ratchet and the energy decay rates for the system are shown to obey the power law for late times, a behavior typical of discrete baths which for low and intermediate values of N always induce a non-Markovian process. The exponential decay is recovered for high bath frequencies distribution and for high values of N, where the Markovian limit is expected. Moreover, by including the external oscillating field with intensity F, we show that current reversal occurs in two situations: By increasing N and by switching from low to high frequencies distribution of the bath. The mobility of particles is shown to have a maximum at $F=0.1$, which is N independent (for higher values of N).

DOI: 10.1103/PhysRevE.78.031126 PACS number(s): 05.40.−a, 05.60.Cd

I. INTRODUCTION

A suitable ingredient for the theoretical description of dissipation is the concept of an open system which interacts with a bath (environment) by collision processes or via other means of energy exchange. The whole problem (system plus environment plus interaction) is conservative but, due to energy exchange between system and environment, the system only can be interpreted as an open system with dissipation. Such microscopic theoretical models have been proposed and used to describe dissipation in classical [1–3] and quantum [3–5] systems and can be applied also in the context of stochastic Schrödinger equations [6–8]. A pleasing example of the application of system-plus-environment models is the description of charge and energy transfer in quantum molecular systems [9].

Different from most of the system (S)-plus-oscillators (O)-plus-interaction (I) models, here the environment is composed by the finite number N of uncoupled harmonic oscillators, characterizing the discrete bath. In the limit of low values of N, the environment power spectrum is not a smooth function but presents strong variations since many frequencies are not present in the interval of interest. The system particle is coupled to the few oscillation modes of the environment. In the limit $N\to\infty$ the discrete bath should approach the continuous bath. To our knowledge the first theoretical attempt to describe a system coupled to a kind of finite bath was done by Mazur *et al.* [10]. They discussed irreversibility in assemblies of coupled harmonic oscillators using time relaxed correlation function.

Discrete baths may present unique features which are not usual in continuous baths. One of these features, which is mainly related to results from the present paper, is the nonexponential and power-law decay of some quantities (for example, energy decay rates, hopping probability, and decoherence). In this context there are a few theoretical papers which consider discrete baths [10–12]. Apparently the main reason to observe the nonexponential and power-law decays rates is the non-Markovian system motion induced by the bath discreteness. In a recent work [13] a complex environment composed of a sum of sub-baths was considered. Each sub-bath is able to induce a Markovian system evolution. However, the system entanglement with different sub-baths induce non-Markovian effects and nonexponential and power-law decays rates are observed. Although this complex environment is not a discrete bath, the sum of smooth sub-baths induces the same process (non-Markovian) as observed by us for discrete baths. Another related result is the subexponential decoherence observed in a two-level system coupled to finite baths [11]. In this paper they consider two kind of discrete baths: One with internal anharmonic couplings and the other one where the baths modes are coupled to other bath modes, but not to the system. Decoherence is fitted by power laws and they showed that the intrabath anharmonic couplings are more effective to recover the exponential dynamics than additional bath modes. In the last theoretical work we mention in this context, the energy-relative fluctuation of a system coupled to a finite bath was treated [12]. They consider two systems: The one-dimensional harmonic oscillators and a chain of N quartic oscillators. In both cases the energy distribution function decays as a power law in N, but any possible relation with (non)-Markovian processes is not analyzed. Other features which are correlated to finite baths, but which are not treated here, is the lost of transport properties in ratchets [14] and the relation between superdiffuse motion (and Levy processes) with the maximal mobility of particles along ratchet devices [15]. We mention some realistic examples where finite and discrete baths are present: Quantum cavities with finite number of frequency modes [16–18]; photon spectral function for excitons [19], where the power spectrum from the bath is continuous but very complicated; electronic two-level systems coupled to a finite set of harmonic vibrational modes [20]; and complex atomic and molecular systems [21–23], where the degrees of freedom of interest are coupled to an environment which can be

highly structured (with the finite number of modes) and may itself exhibit specific features of the dynamical system.

In this paper we integrate numerically $2N+2$ equations of motion from the full conservative problem $(S)+(O)+(I)$. All uncoupled oscillators are coupled indirectly via the system particle. As N increases the system energy is transferred more and more into the finite bath and dissipation effects appear for the integrated times. The system dynamics is a kind of "dissipative reduced dynamics" which mimics the full problem. As a consequence, from the point of view of the nonlinear analysis, our dynamics is simpler than a $2N+2$ high-dimensional conservative system. Usually such high-dimensional systems present all characteristics of complexity [24], which may arise in the interplay between small dissipative and conservative dynamics [24,25]. Even for low-dimensional systems, elliptic periodic orbits become small sinks when small dissipation is added and an infinite number of periodic attractors may coexist [26]. Recently, Ref. [27] showed the relevance of such properties to generate large currents due to the presence of stability islands inside the chaotic sea in the Hamiltonian limit of a dissipative ratchet model. Our goal here is to analyze dissipation (energy lost by the system), the dynamics and the transport in ratchets coupled to the finite bath. From this perspective we are working at the border line between small dissipative and conservative systems. The nonlinear analysis for the $(S)+(O)+(I)$ problem, at this border line, was considered recently by the authors [28]. Ratchet potentials [29] subjected to an external time-dependent field have become an interesting problem due to the possibility to obtain transport properties by extracting usable work from unbiased nonequilibrium fluctuations of the environment. They have been the subject of much research interest because of its relevance in areas of physics [30–32], chemistry [33], and biophysics [34,35]. These references are just reviews in each area, since the actual literature related to ratchets is enormous.

By changing N we will analyze the following: The rate of dissipation (of the system only), the energy transfer dynamics between system and environment, transport and hopping probability between potential wells. There are some interesting questions related to this analysis. How many oscillators are needed to observe dissipation for finite times in the system? How does the dissipation rate decay depend on the number of oscillators? Since the energy transfer dynamics is essential to describe physical processes, how does it depend on the number of oscillators? Is there any optimal transport for a given number of oscillators? The purpose of this paper is to discuss related questions.

The paper is organized as follows: Sections II and III present the model of the finite bath and its main characteristics. While Secs. IV and V discuss the case of no external field, in Sec. VI the external oscillating field is added and the net current along the ratchet is analyzed as a function of N. In Sec. IV the energy transfer dynamics is studied by increasing the number of oscillators. While Sec. IV A treats the intrawell case, Sec. IV B considers the interwell case, where the particle is transferred from one well to another. In Sec. IV C the hopping probability between different wells is shown to obey a power law. Section V discusses the dissipation decay rate as a function of N. Here an ensemble of trajectories is considered and again a power law is found, now for the dissipation decay rate. The exponential decay is recovered for high bath frequencies distribution and for higher values of N. Finally, in Sec. VI the current is studied as a function of N and for different values of the external amplitude. Final remarks containing the main results of this paper are summarized in Sec. VII.

II. MODEL

Let us consider the problem composed by the particle under the influence of an asymmetric periodic potential of the ratchet type (the system) interacting with N-independent harmonic oscillators (the environment). The Hamiltonian of the full problem is given by

$$H = \frac{P^2}{2M} + V(X) + \sum_j^N \left[\frac{p_j^2}{2m_j} + \frac{m_j\omega_j^2}{2}\left(x_j - \frac{\Gamma_j X}{m_j\omega_j^2} \right)^2 \right] - XF_{\text{ext}}(t). \tag{1}$$

Here X and $x_j (j=1,2,\ldots,N)$ are, respectively, system and oscillator coordinates. The coupling parameter Γ_j is the measure of the strength of the system-environment interaction. $F_{\text{ext}}(t)=F_0\cos(\omega_D t)$ is the external force with intensity F_0 and frequency ω_D acting only on the system particle. $V(X)$ is the ratchet potential and is given by [36]

$$V(X) = V_1 - V_0 \sin 2\pi\frac{(X-X_0)}{L} - \frac{V_0}{4}\sin 4\pi\frac{(X-X_0)}{L}, \tag{2}$$

where L is the periodicity of the potential, V_0 is the amplitude, and V_1 is an arbitrary constant. The potential is shifted by an amount X_0 in order to locate one minimum of the ratchet potential at the origin.

Usually in system-plus-environment models the coordinates of the environment can be eliminated resulting in a one-dimensional generalized Langevin equation given by [3]

$$M\ddot{X}(t) + \frac{\partial V(X)}{\partial X} = -\int_0^t d\tau K(t-\tau)\dot{X}(\tau) + f(t) + F_{\text{ext}}(t). \tag{3}$$

The dissipative memory kernel is written as

$$K(t-\tau) = \sum_{j=1}^N \frac{\Gamma_j^2}{m_j\omega_j^2}\cos[\omega_j(t-\tau)], \tag{4}$$

with the fluctuation force

$$f(t) = \sum_{j=1}^N \left[\left(\Gamma_j x_j(0) - \frac{\Gamma_j^2}{m_j\omega_j^2}X(0) \right)\cos(\omega_j t) + \Gamma_j\frac{p_j(0)}{m_j\omega_j}\sin(\omega_j t) \right], \tag{5}$$

which averages to zero. The quantities $K(t-\tau)$ and $f(t)$ contain the whole effect of the N oscillators on the system particle. They depend on the system particle only through $X(0)$. It is possible to write [3]

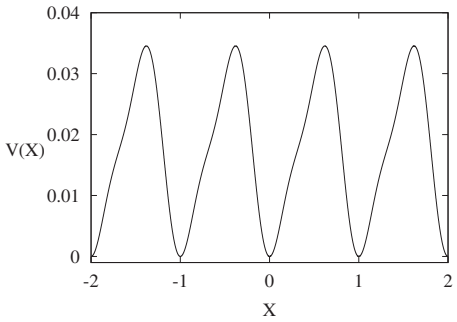

FIG. 1. Dimensionless ratchet potential $V(X)$. The minima of the potential are localized at $X=0, \pm 1, \pm 2, \pm 3, \ldots$.

$$\langle f(t)f(\tau)\rangle = k_B T \sum_{j=1}^{N} \frac{\Gamma_j^2}{m_j \omega_j^2} \cos[\omega_j(t-\tau)] = NC_N(t), \quad (6)$$

which also defines the autocorrelation function $C_N(t)$. From this expression follows the dissipation-fluctuation theorem $\langle f(t)f(\tau)\rangle = k_B TK(t-\tau)$. To notice in such approach is the weak coupling between system and environment and the infinite number of oscillators of the environment characterizing the bath. The dynamics of the system particle is characterized by the continuous spectral density of the bath [2,5], defined by $J(\omega)=\Sigma_j^N \frac{\Gamma_j^2}{m_j\omega_j}\delta(\omega-\omega_j)$.

Different from the above Langevin approach, in this work a finite number of oscillators is considered. In order to do this, we integrated numerically the $2N+2$ first-order equations of motions related to Eq. (1). This is not trivial because very distinct time scales for the system and oscillators may lead to technical numerical problems. To avoid such difficulties, the equations of motions related to Eq. (1) must be written in the dimensionless form. Let us define the following dimensionless units: $X'=X/L$, $X_0'=X_0/L$, $x_j'=x_j/L$, $t'=\omega_0 t$, $\omega_j'=\omega_j/\omega_0$, $\gamma_j=\Gamma_j/M\omega_0^2$, $m_j'=m_j/M$, $F=F_0/ML\omega_0^2$, $\omega=\omega_D/\omega_0$, and $E'=E/(ML^2\omega^2)$ (E is the total energy). The frequency ω_0 is given by $\omega_0^2=4\pi^2V_0\delta/ML^2$ and $\delta=\sin 2\pi|X_0'|+\sin 4\pi|X_0'|$. The frequency ω_0 is the frequency of the linear motion around the minima of the ratchet potential, Eq. (2). After renaming the variables, the dimensionless equations of motion without the primes read as

$$\ddot{X} + \frac{dV(X)}{dX} - \sum_j^N \gamma_j x_j + X\sum_j^N \frac{\gamma_j^2}{m_j\omega_j^2} = F\cos\omega t, \quad (7)$$

$$\ddot{x}_j + \omega_j^2 x_j - \frac{\gamma_j}{m_j}X = 0, \quad (8)$$

where the dimensionless ratchet potential (see Fig. 1) is given by

$$V(X) = C - \frac{1}{4\pi^2\delta}\left(\sin 2\pi(X-X_0) + \frac{1}{4}\sin 4\pi(X-X_0)\right).$$

The constant $C\sim 0.0173$ is such that $V(0)=0$, $X_0\sim -0.19$, and $\delta\sim 1.60$. The dimensionless equations of motion (7) and (8) are the equations analyzed in this work. We used a fourth-order Runge-Kutta integrator [37] with fixed step $\Delta t=10^{-3}$.

For all cases considered in this paper, the dimensionless mass for all oscillators is $m_j=m=0.1$ and the dimensionless coupling $\gamma_j=\gamma$ is also equal for all oscillators. For better visualization of the results, Sec. IV B uses $\gamma=0.03$, while all other sections use $\gamma=0.1$. At times $t=0$, system and environment are not considered to be in equilibrium. The interaction energy is assumed to be zero, the energy of the system is very close to the total energy $E_S\sim E_T$ and the oscillators energy are close to zero, $E_O\sim 0$. The energy in all figures is adimensional and oscillators frequencies are written in units of ω_0. The initial distribution of the oscillators position and velocity is uniform around zero.

III. PROPERTIES OF THE DISCRETE BATH

In order to obtain the particle motion where the frictional force is proportional to the velocity, in this paper we assume the Ohmic bath [5] in the limit $N\to\infty$. The frequencies distribution is then a quadratic (Debye type) with the cutoff at ω_{cut}. For such quadratic frequency distribution the spectral density can be written as $J(\omega\leqslant\omega_{\text{cut}})=\eta\omega$, where η is the viscosity. When the cutoff frequency increases, the viscosity decreases. While the quadratic case is used to analyze the hopping probability (Sec. IV C), energy decay rates (Sec. V) and currents (Sec. VI), the sub-Ohmic, Ohmic, super-Ohmic and nonrandomic cases are discussed in this section.

The properties of the discrete bath depend strongly on the frequencies distribution of the N uncoupled harmonic oscillators. Since $K(t-\tau)$ [Eq. (4)] and $f(t)$ [Eq. (5)] contain the whole effect of the N oscillators on the system particle, in this section we discuss numerically the normalized autocorrelation function $C_N(t)=\frac{1}{N}\langle f(t)f(\tau)\rangle$ from Eq. (6) for different frequencies distributions. In fact we use the dimensionless version of Eq. (6). In the limit of $N\to\infty$ and $t\to\infty$ the autocorrelation function $C_N(t)$ goes to zero for a Markovian process. In such systems $C_N(t)$ decays exponentially ($e^{-\alpha t}$) in time and the correlation time α^{-1} can be interpreted as the collision time [1].

In the Markovian limit, between subsequent collisions we expect to have many oscillations of the bath. Therefore, as we will see, is it almost impossible to reach the Markovian limit when frequencies of the bath are close to zero, even for $N\to\infty$ and $t\to\infty$. For processes with finite values of N the dynamics is much more complicated. In such cases, even for $t\to\infty$, Poincaré recurrence times exist and the value of $C_N(t)$, found at a given time, must be found over and over again. For a discussion about this subject we refer the readers to [10], where the authors discuss the properties of the function $f_N(t)=\Sigma_{j=1}^N\cos(\omega_j t)$ using statistical properties of $\{\omega_j\}$. Different from the present work, they do not employ detailed information about the ω's. In other physical systems (see [19]), the bath can be simultaneously highly structurated and continuous. In such cases the spectral density must be determined appropriately and it is certainly a complicated function of ω. In our approach, due to the finite number of oscillators, the spectral density must be determined numerically and is always structured for low values of N, and depends on

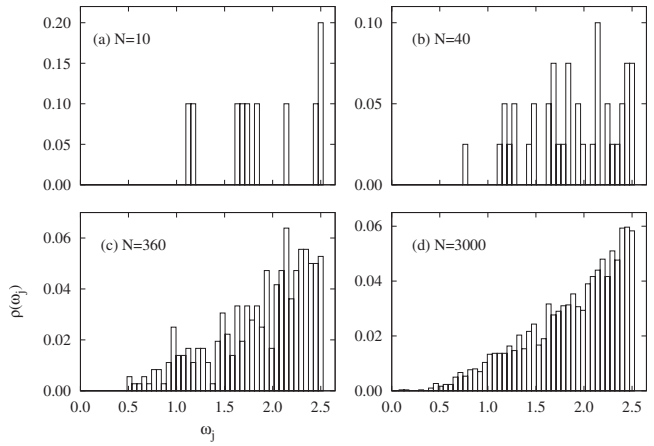

FIG. 2. Frequency distribution for different values of N and $0.0 \lesssim \omega_j \lesssim 2.5$.

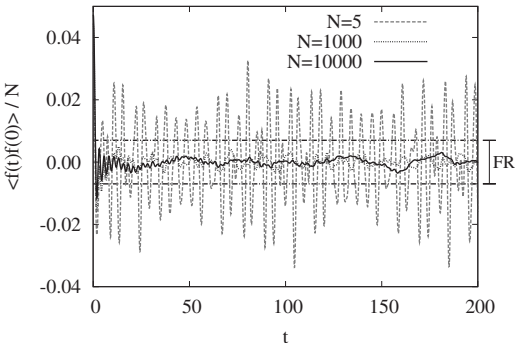

FIG. 3. Normalized correlation function $C_N(t)$ for some values of N and $0.0 \lesssim \omega_j \lesssim 2.5$.

the frequencies generator used in the simulations. However, the qualitative behavior of our results is independent of the frequencies generator.

Next we discuss the autocorrelation function for different bath frequencies distributions. While Secs. III A and III B discuss the quadratic case by changing N and ω_{cut}, respectively, Sec. III C shows results for the sub- and super-Ohmic cases and Sec. III D discuss the nonrandomic case.

A. Quadratic distribution: Increasing N

Figures 2(a) and 2(b) show the distribution $\rho(\omega_j)$ for $N=10$ and $N=40$, respectively. Clearly it can be observed that many frequencies are missing in the interval of interest. This characterizes a highly structured environment, which is a direct consequence of the finite number of oscillators. As the number of oscillators increases to $N=360$ and 3000, $\rho(\omega_j)$ approaches very slowly to a continuous function with a quadratic dependence on ω. The distributions shown in Fig. 2 are given in the interval $0.0 \lesssim \omega_j \lesssim \omega_{\text{cut}}$ ($\Delta\omega_j \sim 2.5$), with the cutoff at $\omega_{\text{cut}}=2.5$. We refer to them as the low distribution. For a later purpose we will refer to the case $\omega_{\text{cut}}=4.0$ ($1.5 \lesssim \omega_j \lesssim 4.0$) as the high distribution. Observe that we always keep $\Delta\omega_j \sim 2.5$ constant. It is also important to mention that in the low distribution the frequency range from the environment includes the system frequency ω_0, i.e., includes $\omega_j \sim 1$. However, in the high distribution all frequencies are larger than ω_0. This will be important in Sec. V.

Figure 3 shows the time dependence of the normalized autocorrelation function $C_N(t)$ for different values of N and $\omega_{\text{cut}}=2.5$. We observe that for low values of N (=5, dashed line), $C_N(t)$ oscillates more or less regularly around zero, without decreasing its amplitude. This means that any value of $C_N(t)$ obtained for a given time, will be repeated over and over again for other times. The time of these repetitions is the Poincaré recurrence time. In other words, the value of $C_N(t)$ at a given time represents the "physical state" of the discrete bath at that time. Therefore we expect that this "physical state" is reached again and again, following the Poincaré times.

As N increases the amplitude of the oscillations of $C_N(t)$ decreases. Compare $N=5$ (dashed line) with $N=1000$ (dotted line) and $N=10\,000$ (full line) in Fig. 3. For times $t \gtrsim 10$, $N=1000$, and $N=10\,000$, $C_N(t)$ starts to oscillate inside the "fluctuation region" (FR) [10]. This region is shown in Fig. 3 with two horizontal straight lines. In such cases, $C_N(t)$ decays initially very fast and then remains inside the FR. For values of $C_N(t)$ inside the FR region (for $t \gtrsim 10$ in Fig. 3), the Poincaré recurrence times are small and $C_N(t)$ is repeated over and over again. States of the discrete bath related to these times can be named "probable states" [10], since they appear very often. For values of $C_N(t)$ outside the FR region (for $t \sim 0.0$ in Fig. 3, for example), Poincaré recurrence times are enormously large and it is very difficult to observe the repetition of such values of $C_N(t)$ for the finite integration times. States of the discrete bath related to these times can be named "improbable states." For large values of N the initial states from Fig. 3 ($t \sim 0.0$) belong to such improbable states.

For Markovian processes the FR should go to zero for $N \to \infty$ and $t \to \infty$. Therefore, from the analysis of this section we say that the dynamics of the system coupled to the discrete bath with low frequencies is almost a non-Markovian process, independent of N.

B. Quadratic distribution: Going to higher frequencies

In this section we study the autocorrelation function by increasing the cutoff frequency. In fact we "move" the distribution to higher frequencies keeping the frequency interval fixed by $\Delta\omega_j \sim 2.5$. We use values of $N=10, 20, 50, 100, 1000, 10\,000$. The qualitative behavior of $\rho(\omega_j)$ and the frequencies generator are exactly the same as in Sec. III A. Figure 4 shows the semilogarithmic plot of the FR as a function of ω_{cut} for different values of N. In all of the following simulations we determined the FR using the time interval $\Delta t=[400, 50\,000]$, independent of N. Therefore, we extracted an initial transient of around 400. The choice if this time interval allows us to obtain all relevant variations of FR. In Fig. 4 we observe that the FR decreases when the ω_{cut} increases, meaning that the Markovian limit could be reached by increasing the mean bath frequencies. We also observe the expected result that the FR decreases when N increases. In general the autocorrelation function goes to zero for higher frequencies and for $N \to \infty$. Only in this limit

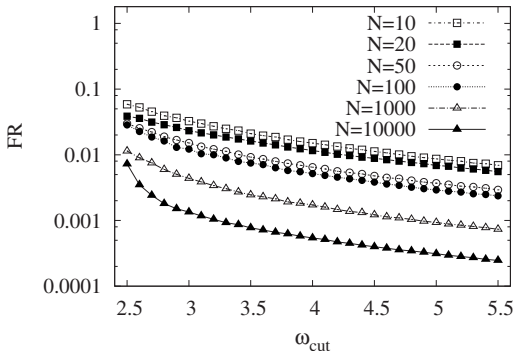

FIG. 4. Fluctuation range as a function of ω_{cut} for $s=1$.

our discrete bath behaves like an usual Markovian Ohmic heat bath. Any bath discreteness induces finite values for the FR and, consequently, the non-Markovian motion.

In this section we discussed the case when the distribution "moves" to higher frequencies keeping the frequency interval fixed by $\Delta\omega_j \sim 2.5$. We could obviously discuss the case when only ω_{cut} increases keeping the lower frequency close to zero. However, if we do so, for any new value of ω_{cut} the interval $\Delta\omega_j$ increases and the discreteness of the bath changes, i.e., the density of frequencies will decrease as ω_{cut} increases. Since our interest is to study the dynamics by increasing N, without decreasing the frequency density, we do not discuss this case here.

C. From sub-Ohmic to super-Ohmic baths

To discuss the bath discreteness for other types of distributions, we consider the cases for which the spectral density has the form $J(\omega)=\omega^s$, with $0<s\leqslant 2$ [5]. For $s=1$ the quadratic frequency distribution discussed above is recovered. For $s<1$ we have the sub-Ohmic case where lower frequencies in the allowed frequency interval have a bigger contribution when $N\to\infty$. For $s>1$ we have the super-Ohmic case where higher frequencies in the allowed frequency interval have a larger contribution when $N\to\infty$. Nonintegral values of s correspond to fractal environments [5]. Figure 5 shows the semilogarithmic plot of the FR as a function of s for different values of N and $\omega_{\text{cut}}=2.5$. In general the FR decreases as s increases, showing that the super-Ohmic case is

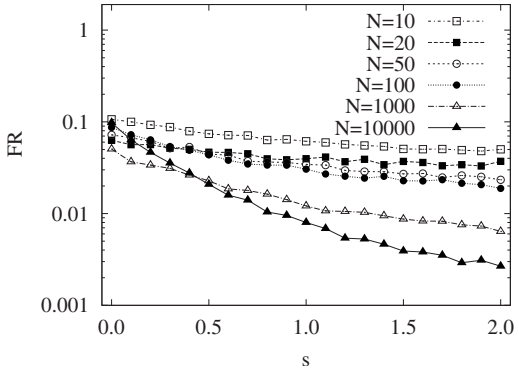

FIG. 5. Fluctuation range as a function of s for the low distribution $0.0\leqslant\omega_j\leqslant 2.5$.

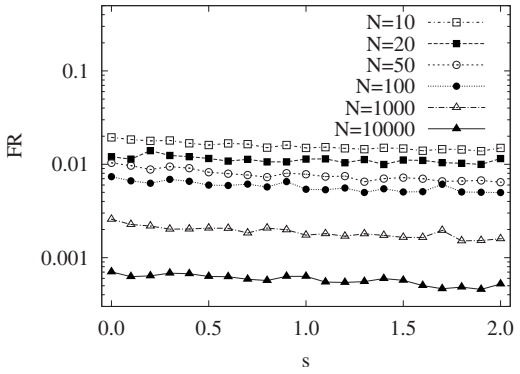

FIG. 6. Fluctuation range as a function of s for the high distribution $1.5\leqslant\omega_j\leqslant 4.0$.

"more Markovian" than the sub-Ohmic case. Besides $N=1000, 10\,000$, all other curves have the same qualitative s dependence. The reason for this distinct behavior is the consequence of frequencies close to zero. Since the interval of allowed bath frequencies is $0.0\leqslant\omega_j\leqslant 2.5$, when N increases from 100 to 10 000, the number of frequencies close to zero increases significantly. These close to zero frequencies make the FR increase, the motion is strongly non-Markovian and the qualitative behavior of FR as a function of s changes. We observe that for $s\leqslant 0.5$, all of the values of the FR for $N=10\,000$ are higher when compared to $N=1000$. Since in the sub-Ohmic distribution lower frequencies have a larger contribution, means that close to zero frequencies become more probable to occur. As a consequence the values of FR increase very much when s decreases. These close to zero frequencies change the qualitative behavior of the FR for $N=100, 10\,000$.

As the cutoff frequency increases, the zero frequencies are not present anymore and the above distinct effect observed for $N=100\to 10\,000$ should disappear. Figure 6 shows the FR as a function of s when $\omega_{\text{cut}}\sim 4.0$. Clearly we realize that the FR now decreases in the transition $N=100\to 10\,000$, showing that the anomalous effect due to the zero frequencies disappears Different from Fig. 5, here the FR is almost s independent, but still N dependent.

D. Nonrandomic distributions

Nothing essentially new occurs for nonrandomic distributions when compared to the last two sections. Basically, as before, the autocorrelation function goes to zero for $N\to\infty$, $t\to\infty$ and for higher distributions. If we consider equally spaced frequencies, for example, at some specific times (the Poincaré recurrence times) we observe the constructive interference (full recurrences) of the autocorrelation function. The autocorrelation function has well-defined peaks at well-defined times. As N increases, the maxima of these peaks decrease and the times for full recurrences increase. Between these well time localized peaks the autocorrelation function approaches zero as $N\to\infty$. Physically this example could correspond to the system coupled to a classical resonator where a discrete number of modes is allowed (the discrete bath). The modes are usually integer multiples of the funda-

mental frequency. From the quantum point of view this could correspond to the interaction of atomic levels with a quantum cavity composed of finite modes [16].

IV. ENERGY TRANSFER DYNAMICS ($F=0$)

There are two distinct physical situations where the energy transfer can be discussed: (i) The energy redistribution between system, environment, and interaction in case the particle stays inside one ratchet potential well, and (ii) the energy redistribution in case the particle is transferred from one ratchet potential well to another. These situations can be interpreted, respectively, as the classical analogous of the much more complicated quantum dynamics, for example, the intramolecular redistribution and intermolecular charge transfer [9]. The particle staying inside one ratchet potential well would correspond to the charge staying inside one molecule. The particle being transferred from one ratchet potential well to another, would correspond to the charge being transferred from one molecule to another. Because of the analogy, the above two physical situation are called here the intrawell energy redistribution and the interwell particle transfer, respectively. This is just an analogy and it is not our intention to connect the classical results with the quantum problem of molecules mentioned above.

In this section the two distinct physical situations mentioned above are briefly discussed. To do so, energy exchange from just one trajectory and one environment realization is considered in Secs. IV A and IV B. In Sec. IV C the hopping probability is analyzed over 800 environment realizations. We used low distributions for the environment frequencies in Sec. IV A and IV B, and high distributions in Sec. IV C.

A. Intrawell energy redistribution

Initial conditions for the particle are $X(0)=0.0$, $\dot{X}(0)=0.2$, and the scaled coupling is $\gamma_j=0.1$. For $1\leqslant N\leqslant 10$ the system particle is continuously exchanging energy with the finite bath. Essentially the particle is oscillating inside one ratchet potential well keeping for itself most of the total energy with little variations.

Figures 7(a) and 7(b) show the case of the system-plus-15 oscillators. The frequency (for times $t\leqslant 670$) of the energy exchange between system and environment is $\omega_{\text{slow}}\sim 0.035$. Different from the cases with low values of N, near $t\sim 670$ the system abruptly loses one-half of its energy to the environment [mostly to the oscillators with lower frequencies, see Fig. 7(b)]. The initial energy lost by the particle is not fed back for the integrated time and dissipation effects appear. It is obvious that if we integrate until $t\to\infty$ the energy must return to the particle due to the finite bath and the Poincaré recurrence times. However, since in the real world we are always restricted to finite times, the dissipation process described in this section is of real interest.

For $N\to\infty$ the system energy should be mostly transferred to the environment, and only fluctuations are expected. This can be observed in Fig. 8 for $N=360$. After reaching the limit situation of equilibrium (at $t\sim 1100$), system and environment exchange energy while the interaction energy is close to zero. As expected, for an environment composed of many oscillators, most of the energy is transferred from the system into the environment. The frequency of the energy exchange between E_S and E_O is not well defined and only fluctuations in E_S are observed. Following the discussion of Sec. III A, we can mention that the system states at $t\lesssim 1100$ are improbable states with very large Poincaré recurrence times, while the states for $1100\lesssim t\lesssim 15\times 10^3$ are the probable states with small Poincaré times.

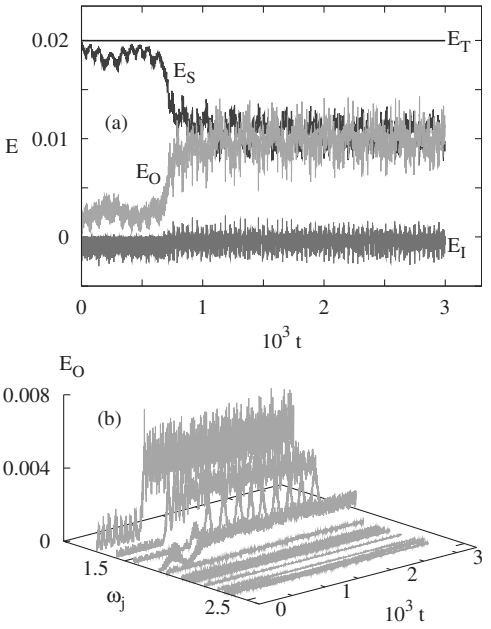

FIG. 7. Time evolution of separated energies: (a) The system E_S, oscillators E_O, interaction E_I, and total E_T for $N=15$ oscillators and (b) details of the energy for each of the 15 oscillators.

B. Interwell particle transfer

Another aspect of the energy transfer dynamics occurs in cases when the particle is transferred from one ratchet potential well to another. At $t=0$ the particle receives enough energy ($E_S\sim 0.0346$) to transpose the peak of the ratchet barrier, with potential energy close to ~ 0.0323. As it moves over the ratchet potential wells, it will "fall" into one ratchet

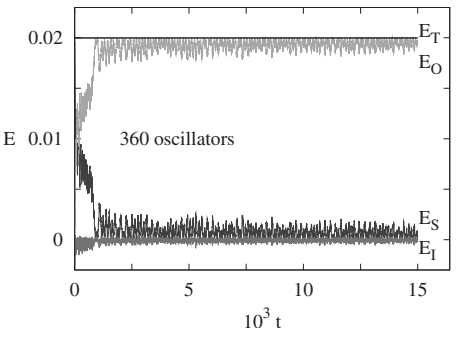

FIG. 8. Time evolution of separated energies: The system E_S, oscillators E_O, interaction E_I, and total E_T for $N=360$ oscillators.

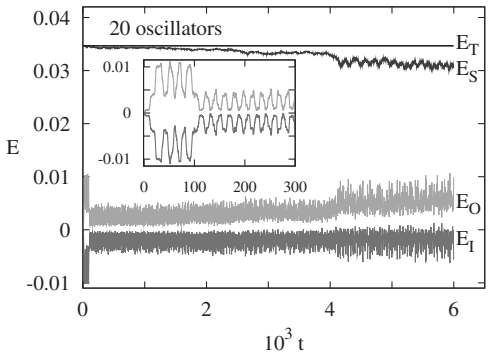

FIG. 9. Time evolution of separated energies: The system E_S, oscillators E_O, interaction E_I, and total E_T for the case of the transferred particle and $N=20$.

well due to damping and dissipation effects. For illustrative purposes the scaled coupling considered here is weaker ($\gamma_j=0.03$), and the initial conditions for the particle are $X(0)=0.0$ and $\dot{X}(0)=0.263$.

In Fig. 9 the time evolution of the energies is shown for the case of $N=20$ oscillators. The initial energy is assumed to be higher when compared with the preceding section, and the particle will transpose (to the right) two ratchet potential barriers. Since the coupling strength between system and environment is weaker, dissipation effects are expected to appear only for longer times. The integrated time for Fig. 9 is therefore longer. All other parameters are the same as from the preceding section. The inset of Fig. 9 shows details of environment and interaction energies for $t \lesssim 300$.

In order to discuss better the energy transfer dynamics, it is important to look simultaneously at what happens to the trajectory in position and phase space, shown in Fig. 10. For times $0.0 \lesssim t \lesssim 22$, the particle moves to the right [$\dot{X}(0) > 0.0$] over two ratchet potential wells (remember, the period of the ratchet wells is 1.0) and, due to dissipation effects of the 20 oscillators, it "falls" into the well localized around the minimum $X=2.0$ and oscillates there for times $22 \lesssim t \lesssim 101$. As the particle jumps over the two ratchet wells, energy is stored into the environment which is now in a kind of "excited state" with mean energy around 0.0075. This can be observed in the inset of Fig. 9 for $t \lesssim 101$. The same happens

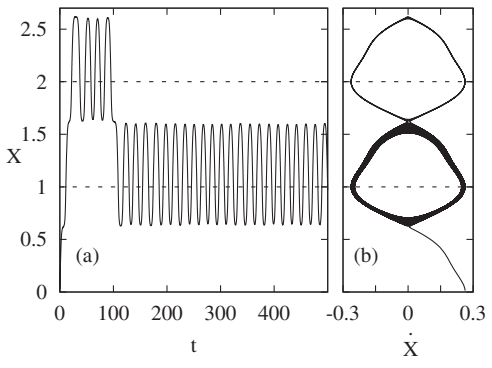

FIG. 10. Phase-space trajectory for $N=20$ showing (a) time dependence of the position of the particles and (b) the trajectory in phase space.

for the interaction energy but for negative values. For $t \sim 101$ the energy stored in the environment is transferred back to the particle and it jumps back (to the left) one ratchet well, oscillating around $X=1.0$ and staying there for the whole integrated time (see Fig. 10).

As the particle jumps back the last one ratchet well, the environment decays to the "lower excited state" with mean energy around 0.0025. See the environment energy for $t \gtrsim 101$ in the inset of Fig. 9. This remaining energy inside the environment is not enough to make the particle jump another ratchet well. Therefore, the particle stays inside the ratchet well centered around $X=1.0$ for the whole integrated time. For times $101 \lesssim t < 6 \times 10^3$, the system energy is slowly transferred into the environment. As a consequence, the particle inside the ratchet well is slowly losing its energy, which is manifested by the width of the trajectory in Fig. 10(b).

For $1 \leqslant N \lesssim 27$ the environment affects the particle through two different processes. First, the environment is damping the motion of the particle, making it "to fall" into the ratchet potential well and to stay there for a brief time. Remember that for $t=0$ the particle received enough kinetic energy to transpose the ratchet barrier. Second, the environment may inject energy back into the system, transferring the particle from one ratchet well to another. This is called the "jump effect" or environment-induced transfer. For the same trajectory this effect may occur many times. Increasing the number of oscillators the "jump effect" will disappear (for $N \gtrsim 27$) and only dissipation and damping effects remain. So, only for $N \gtrsim 27$ the particle will lose enough energy to the environment in order to "fall" into one ratchet potential well, staying there for the whole integrated time.

C. Hopping probability

Although results from the preceding section are shown for just one trajectory, the effect of the environment-induced particle transfer is observed for many trajectories and is a common phenomenum for low values of N. This is shown in this section by calculating the hopping probability between many wells. Due to the environment-induced transfer, particles may jump to the right and to the left. Since we have many wells, an adequate way of quantifying the hopping probability is to count how many times $n_r(n_l)$ the particle jumps to a right (left) ratchet well. The quantity n_r/n_t (n_l/n_t) gives us the normalized number of right (left) jumps, where $n_t=n_r+n_l$. This way of quantifying the movement of particles allows us to analyze the decay of the hopping probability along the whole periodic structure.

Figure 11 shows the distribution of the right jump probability $\rho(n_r)$ after an integration time up to $t=5000$ and over 800 realizations of the environment variables. Initial conditions for the particle are $X(0)=0.0$ and $\dot{X}(0)=0.2633$, the coupling is $\gamma_j=0.1$, and the high distribution is used. The idea here is to observe the effect of the finite environment on the motion of the particle which initially has enough kinetic energy to transpose all ratchets potentials. For $N=0$ (no environment), for example, we suppose that the particle has enough kinetic energy to transpose the first ratchet well [to the right, since $\dot{X}(0)>0$]. As a consequence, it will transpose

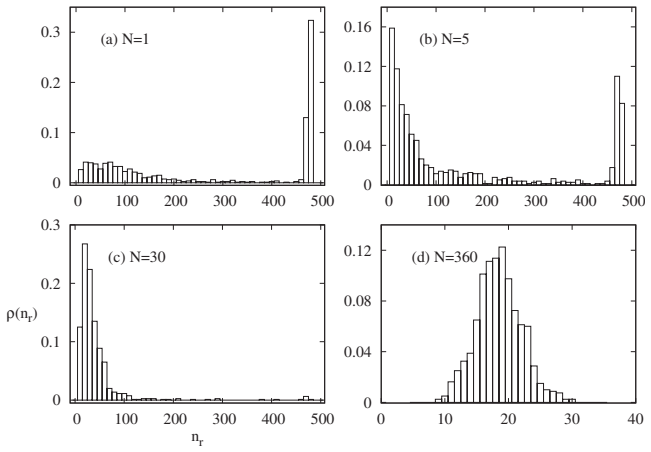

FIG. 11. Distribution of the right jump probability for (a) $N=1$, (b) $N=5$, (c) $N=30$, and (d) $N=360$.

all wells since no dissipation and damping effects are present. For the integrated time and for each realization, the particle transposed 494 ratchet wells, i.e., the particle reached $X(5000)\sim 494$. Therefore, for $N=0$ we have $n_r=494$ and $n_l=0$ for each realization. Now, take the particle above (same initial conditions and same integrated time) but with $N=1$. In this case, the particle may lose part of its kinetic energy due to the "collisions with the environment composed of one oscillator." As a consequence, for some realizations the particle may not reach $X\sim 494$ as before. This is shown in Fig. 11(a), where the pronounced peak with probability ~ 0.3 is observed near $n_r=494$ ($X\sim 494$). It means that most of the trajectories are still jumping to the right over 494 wells. Such a big number of right jumps is obvious because damping and dissipation effects are expected to be small for $N=1$, and the particle is more or less "free" to move over the ratchet wells. We also see in Fig. 11(a) some finite probabilities along lower values of right jumps ($0<n_r\lesssim 200$). Such low values of n_r cannot be a consequence of dissipation and damping effects, because they are small for $N=1$. Low values of n_r are the consequence of left jumps, or the environment-induced transfer observed in the preceding section. For $N=5$, dissipation and damping effects start to affect more the dynamics, and the number of initial conditions which reach $X\sim 494$ is lower [see Fig. 11(b)]. As the number of oscillators increase to $N=30$ [Fig. 11(c)], damping and dissipation start to be stronger, environment-induced transfers get smaller, and the final right jump probability approximates (for $N=360$) a kind of Gaussian distribution around $n_r\sim 20$ wells [see Fig. 11(d)].

A more qualitative way to observe this is to study the total right $P_r(N)$ [or left $P_l(N)$] normalized jump probabilities as a function of N. They are obtained by simply adding, for a given N, all values of n_r (or n_l) over the 800 realizations, and dividing them by 494×800, which is the maximal value of $n_r\times 800$ obtained for $N=0$. Figure 12 shows $P_r(N)$ and $P_l(N)$ as a function of N. Both normalized probabilities decrease very fast as N increases. However, the left jump probability, consequence of the environment-induced transfer, decreases much faster and for $N\sim 30$ it is close to zero, as expected from results of the preceding section. We fitted both curves

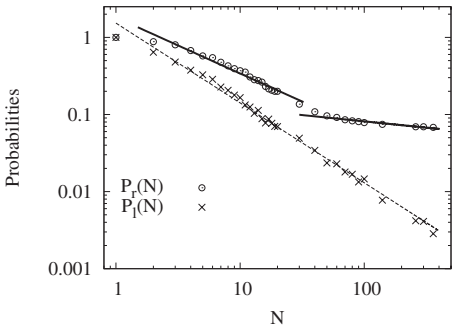

FIG. 12. Total left (×) and right (○) normalized jump probabilities. Dashed and solid lines are the corresponding fitted curves.

by an inverse power law. It can be observed that $P_l(N)$ is well fitted (dashed line) by an inverse power law which goes with exponent ~ 1.04. For $P_r(N)$ however, we clearly see two distinct regions where the exponent of the power law is different. The first for $1<N\lesssim 30$, obeys the inverse power law with exponent ~ 0.635 and the second region, for $N\gtrsim 40$, follows a power law with exponent ~ 0.163. This means that for $1<N\lesssim 30$ the right jump probability $P_r(N)$ is mainly affected by the left jump probability $P_l(N)$, i.e., the environment-induced transfer to the left. As we have shown in the preceding section, this is a typical characteristic of discrete baths. In the region $N\gtrsim 40$, $P_r(N)$ is affected by real damping and dissipation effects.

Concluding this part we showed that, for the given particle with initial velocity (to the right) and 800 environment realizations, the left jump probability vanishes as N increases, showing that the environment-induced transfer (to the left) is destroyed for higher values of N. Moreover, we showed that the right jump probability also decreases as N increases, and that for $N=360$ it has a stationary Gaussian distribution along the periodic structure. For future reference, we call to attention that for $N=360$ the transport of particles along the periodic structure can be destroyed by damping and dissipation, while for low values of N, environment-induced transport is also important. Similar results from this section are obtained when we start with the negative velocity $\dot{X}=-0.2633$. Just change n_r by n_l, and vice versa. It is also worth mentioning that $1/N$ plays the role of the bath temperature T. Since the total energy is equal in all simulations, the mean energy and oscillator from the discrete bath will decrease with N, which corresponds to a bath that becomes colder. Therefore, our escape rate decreases with a power law in ($N\propto 1/T$) while the usual escape rate [5] decreases exponentially with $(1/T)$.

V. ENVIRONMENT-DEPENDENT RATE OF DISSIPATION ($F=0$)

Although the results from Secs. IV A and IV B are important to describe energy transfer dynamics for particular trajectories, they are not sufficient to make statements about general laws of the energy transfer dynamics. In order to do this, in this section the energy transferred from system to environment is studied for an ensemble of particles for the

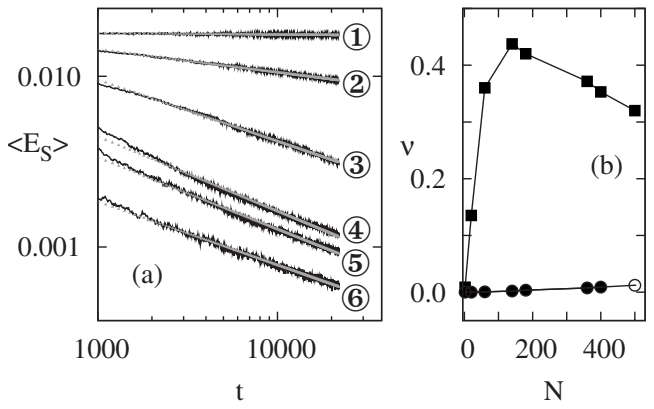

FIG. 13. (a) Log-log plot of the time evolution of averaged system energies (over 800 trajectories) and adjusted curves for $N=2$(①), 20(②), 60(③), 140(④) 180(⑤) and 360(⑥) and (b) values of the exponent ν from Eq. (9) for low distribution (squares), and high distribution (circles).

intrawell case from Sec. IV A. An average over 800 trajectories is taken. The rate of energy lost by the system is analyzed as N increases. The scaled coupling between system and environment is $\gamma_j=0.1$.

Figure 13(a) shows the log-log plot of the time evolution of the average system energy $\langle E_S\rangle$ for different values of N. Only late times ($t>1000$) are discussed. For $N=2$, no decay is observed for the mean system energy and dissipation is considered zero. For $N\geqslant 20$ decay is observed in all cases. We checked the energy decay (over many initial conditions) for all values of $N<20$ and observed that dissipation effects always appear in the interval $10\leqslant N\leqslant 20$. This also agrees with results from the preceding section where dissipation effects start to appear for about $N\sim 15$. The goal now is to find the time decay law for the system dissipation rate for late times. Figure 13(a) shows that the average of the decay rate is linear in the log-log plot. Therefore, the system energy can be well adjusted by an inverse power-law curve given by

$$\langle E_S\rangle \propto t^{-\nu}, \tag{9}$$

where ν is the exponent which determines the dissipation rate. In Fig. 13(a) the adjusted curves are plotted for each value of N, demonstrating that the dissipation decay rates really obeys an inverse power law. The dependence of $\nu(N)$ for the low distribution is shown in Fig. 13(b) (square points). It can be observed that the dissipation decay rate increases as the number of oscillators increases from $N=2$ to $N=140$. In this interval, the energy flows faster from the system into the environment as N increases. For $N=140$, the energy decay rate reaches a maximum and decreases a little for $N=180$, approaching a value near 0.31 for $N=500$. The maximum observed for $N=140$ means that, for this number of oscillators, the environment receives more likely the energy from the system. Such an effect is related to the low distribution which includes values of $\omega_j\leqslant 1$. To explain this we must call to attention that the rate of transferred energy is higher for $\omega_j<1$ than for $\omega_j>1$. This is obvious when we realize that the transferred energy $E_S\rightarrow E_j$ (energy of the jth oscillator) occurs more likely when $E_S>E_j$. Since the low

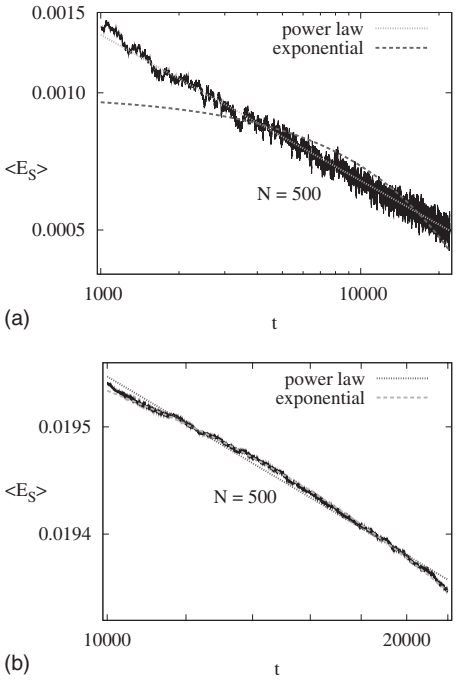

FIG. 14. Log-log plot of the time evolution of averaged system energies and adjusted curves for $N=500$ and (a) low distribution and (b) high distribution. Black lines are results for the simulations, dashed lines for the power-law fit, and long dashed line for the exponential fit.

distribution includes some frequencies with $\omega_j\leqslant 1$, the number of oscillators with $\omega_j<1$ can be different than the number of oscillators with $\omega_j>1$ (for sufficiently low values of N). In fact, it will depend on the frequency generator. A more detailed analysis of the low frequencies distribution showed that the number of oscillators with $\omega_j<1$ are proportionally greater for $N=140$ than for $N=180$ and $N=360$. As a consequence, the rate of the transferred energy is expected to be higher for $N=140$, as observed in Fig. 13(b). When another frequency generator is used, the maximum observed for $N=140$ could occur for other values of N. However, such maximum will only appear for finite baths. The above maximum will disappear when all oscillator frequencies obey $\omega_j>1$. The points (circles) from Fig. 13(b) exemplifies this. It shows the values of ν [from Eq. (9)] as a function of N for the high distribution ($1.5\leqslant\omega_j\leqslant 4.0$). In this case the value of the exponent is close to zero and increases very slowly with N. Therefore, energy decay rates are higher in the low distribution case. The empty circle in Fig. 13(b) for $N=500$ is explained below.

Comparing the above results with the analysis of discrete baths from Sec. III, we conclude that we have two reasons why we see the energy power-law decay: (1) The cutoff frequency distribution is too small and/or (2) the values of N are not large enough. In order to check this we show in Fig. 14 more details of the energy decay for $N=500$ for the low [Fig. 14(a)] and high [Fig. 14(b)] distribution cases. Black lines are results for the simulations, dashed lines for the power-law fit, and long dashed line for the exponential fit. While for the low distribution we still have a power-law, for the high distribution case the energy decay starts to approach an ex-

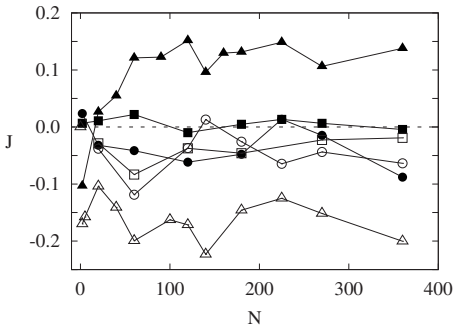

FIG. 15. Current J as a function of N for different values of the amplitude of the external force: $F=0.05$ (□,■), $F=0.1$ (▲,△), $F=0.5$ (●,○). Filled symbols for the low distribution (which includes $\omega_j \leqslant 1.0$ and with $\omega_{\text{cut}} \sim 2.5$), and empty symbols for the high distribution (where all $\omega_j > 1.0$ and $\omega_{\text{cut}} \sim 4.0$).

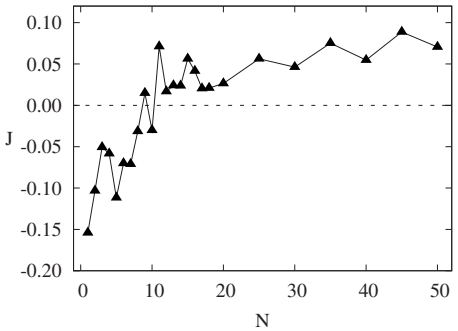

FIG. 16. Current reversal obtained as a function of N. This curve shows in more details the result from Fig. 15 for $F=0.1$.

ponential decay. This transition from power-law to exponential energy decay occurs very slowly and only when the fit is done for later times. Observe that the time interval for the fits from Figs. 14(a) and 14(b) is different. In fact, when we fit the energy decay for the low distribution [Fig. 14(a)], but using later times ($t > 10\,000$), we still get the power law. This is not shown. However, for the high distribution case the differences between the power law and exponential curves in Fig. 14(b) are very small, but convincing. The last point (empty circle) in Fig. 13(b) for $N=500$ comes from the power-law fit from Fig. 14(b). In fact, for this point we should already use the exponential decay, but the differences between both are very small. The main point is that for higher distributions and later times the exponential decay is slowly recovered. As the number N increases the computer CPU times for simulations increases very much. This is the reason we did not consider higher values of N.

For short times ($t < 1000$), a kind of stretched exponential decay rates were found. However, since in our analysis we always start at $t=0$ with a nonequilibrium situation, such decay rates are not discussed here.

VI. CURRENT ($F \neq 0$)

Finally we discuss the transport along the periodic structure by turning on the external force F. The asymmetry of the ratchet potential, together with the external force, allow particles to move in a preference direction inducing the net current. In this section we analyze the current as a function of the number of oscillators. A high efficiency of the current in the ratchet device is a very desirable quantity, then it will affect directly the transport.

The current J along the ratchet can be defined as the time average of the average velocity over an ensemble of initial conditions. It is calculated from $J=\frac{1}{M}\Sigma_{i=1}^{M} v_i$, where the sum is over M different times t_i and v_i is the average velocity at the time t_i over the 800 initial conditions. Figure 15 shows the current as a function of N for different values of the amplitude of the external force $F=0.05$ (□,■), $F=0.1$ (▲,△), $F=0.5$ (●,○). Filled symbols are results for the low distribution and empty symbols are results for the high distribution. The coupling intensity is $\gamma_j=0.1$ and the frequency of the external field is $\omega=0.035$.

First observation in Fig. 15 is that the most relevant currents occur, for both distributions, at $F=0.1$. For $N=2$ these currents are negative [see the (▲,△) points]. As N increases, the current for the high distribution keeps its values inside the interval $(-0.1,-0.2)$. For the low distribution case we observe current reversal occurring in the interval $5 \lesssim N \lesssim 30$. This is shown in more details in Fig. 16. This interval is approximately the interval for which dissipation and bath-induced transfer effects from Secs. IV B and IV C appear (see text related to Fig. 9). Since the environment can induce transfer in another direction than the original, the average over the velocity decreases and the current also decreases. In fact, environment-induced transfer may decreases the efficiency of the current. In our case we can say that the bath-induced particle transfer decreases the current in the interval $2 \lesssim N \lesssim 20$ and contributes for the current reversal. The phenomenon of current reversal is common to appear in ratchets when parameters such as the particle mass, viscosity, amplitude of the external force, and temperature are varied [38,39]. We show here that current reversal occurs when N increases.

Another interesting observation from Fig. 15 is the saturation effect. For $F=0.05$ the current is almost zero for any N, it increases until the maximum is reached at $F=0.1$ (we calculated the current for other intermediate values) and then J returns to be close to zero for higher values of F. This is shown more clearly in Fig. 17, where the current is plotted as a function of F for different values of N. In other words, the mobility of particles, which can be defined as J/F, has a maximum at $F=0.1$. Such saturation as a function of the external amplitude was also observed in the usual treatment of ratchets using the Langevin approach [38–40]. At the maxima $F=0.1$, current reversal is observed by changing from low to high distributions (compare black and gray circles in Fig. 17). Just for comparison, the (×) points plotted in Fig. 17(d) are results obtained by integrating the Langevin equation. The dissipation coefficient used in the Langevin simulation is obtained from the high distribution case from Fig. 13(b).

VII. CONCLUSIONS

While the transport of Brownian particles in periodic structures has been the subject of interest in many areas

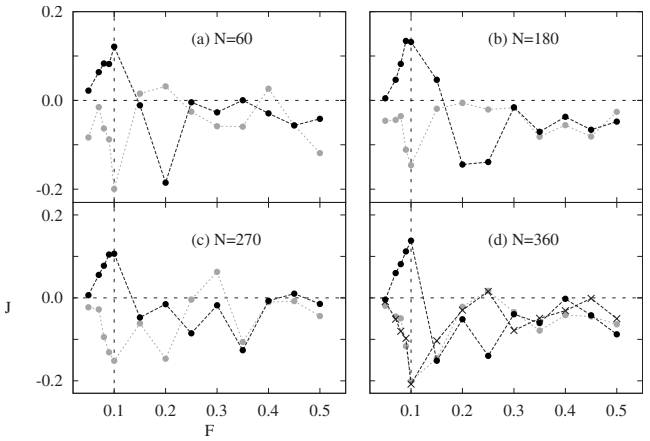

FIG. 17. Current J as a function of the external amplitude F for different values of N. Black (gray) circles are results for the low (high) distribution. The points $\times$ in (d) are results using the Langevin equation.

[30–35], system-plus-environment models have also become popular due to their ability to describe dissipation in classical [1–3] and quantum mechanics [3–6,9]. Usually in such models the environment is well described by the thermal bath composed of infinite uncoupled harmonic oscillators. However, as mentioned in the introduction, there is a reasonable number of systems in nature which are coupled to finite baths [16–19,21,22]. This work analyzes the situation of particles in a ratchet (the system) coupled to the finite number N of oscillators (the discrete bath). In particular, we study the effect of changing N on the transport of particles and hopping probabilities along the ratchet; the energy transfer dynamics between system and the discrete bath; and the dissipation rate of the system.

In Sec. III we discuss the autocorrelation function for different bath frequencies distributions. While Secs. III A and III B discuss the quadratic case by changing N and ω_{cut}, respectively, Sec. III C shows results for the sub- and super-Ohmic cases and Sec. III D discuss the nonrandomic case. The main observation is that the fluctuation range (FR) from the autocorrelation function goes to zero only for higher distributions and for $N \to \infty$. This suggests that the Markovian limit cannot be obtained for discrete baths with low values of N and low distributions.

For the intrawell case, discussed in Sec. IV A, the particle stays inside one ratchet potential well and first manifestation of dissipation were observed for environments composed of $10 \lesssim N \lesssim 20$ oscillators. For lower values of N the initial energy is always fed back into the system, which is the consequence of small Poincaré recurrence times. As the number of oscillators increases, dissipation and damping effects become stronger and most of the system energy is transferred into the environment and only fluctuations in the system energy remain. This is confirmed by results shown in Fig. 8 for $N = 360$. The relation of such results with specific properties of the finite bath (such as the Poincaré recurrence times) was also discussed.

An interesting situation appears for low values of N in the interwell case, where the particle has enough energy to jump over the periodic barriers. Each time the particle jumps over one ratchet barrier, moving away from (closer to) the initial ratchet well, the mean energy of the environment increases (decreases). The environment is in a kind of "excited state." This stored energy in the environment is used to transfer the particle back from one ratchet well to another. An environment-induced particle transfer is observed. For low values of N the environment acts (for the intrawell and interwell cases) actively on the system by transferring enough energy to the particle in order to change qualitatively its motion. This effect will disappear as the number of oscillators increases ($N \gtrsim 27$) and only dissipation and damping effects will remain. Results for the hopping probabilities along the ratchet confirm these results. The total right and left jump probabilities decrease as N increases. Important to mention is that for $N \gtrsim 30$ the transport of particles along the periodic structure is destroyed due to damping and dissipation, while in the case of low values of N ($1 < N \lesssim 27$), the transport is affected by the environment-induced transfer. We mention that this is only possible in finite environments. For an ensemble of particles the dissipation decay rate is shown to obey, for the low and high distributions, an inverse power law for late times. This behavior is typical of discrete baths which for low and intermediate values of N is always non-Markovian. The exponential decay is recovered for high bath frequencies distribution and for high values of N, where the Markovian limit is expected.

Finally we discussed the case of net current induced by the additional external oscillating field with intensity F. The current along the ratchet is studied as a function of N and for different values of F. We showed that a maximum in the mobility of the particles is obtained for $F = 0.1$ for both, low and high distributions. This result is independent of N for $N \gtrsim 27$. For the low distribution case and $F = 0.1$, decreasing the values of N the current decreases, changes its sign, and current reversal is observed. Therefore, when the system is coupled to the modulated environment the mobility of particles may change its direction. Current reversal is also found (for $F = 0.1$) by switching from low to high distribution in the environment.

ACKNOWLEDGMENTS

J.R. and M.W.B. thank CNPq and FINEP, under project CTINFRA-1, for financial support and J. A. O. Freire for helpful discussions.

[1] P. Ullersma, Physica (Utrecht) **32**, 27 (1966).
[2] R. Zwanzig, J. Stat. Phys. **9**, 215 (1973).
[3] E. Cortés, B. J. West, and K. Lindenberg, J. Chem. Phys. **82**, 2708 (1985).
[4] A. O. Caldeira and A. J. Leggett, Phys. Rev. Lett. **46**, 211 (1981).
[5] U. Weiss, *Quantum Dissipative Systems* (World Scientific, Singapore, 1999).
[6] N. G. van Kampen, *Stochastic Processes in Physics and Chemistry* (North-Holland, Amsterdam, 1992).
[7] H. J. Carmichael, *Statistical Methods in Quantum Optics I* (Springer, Berlin, 1999).
[8] W. T. Strunz, L. Diósi, N. Gisin, and T. Yu, Phys. Rev. Lett. **83**, 4909 (1999).
[9] V. May and O. Kühn, *Charge and Energy Transfer Dynamics in Molecular Systems* (Wiley-VCH, Berlin, 2000).
[10] P. Mazur and E. Montroll, J. Math. Phys. **1**, 70 (1960).
[11] V. Wong and M. Gruebele, Chem. Phys. **284**, 29 (2002).
[12] F. Q. Potiguar and U. M. S. Costa, Physica A **342**, 145 (2004).
[13] A. A. Budini, Phys. Rev. E **72**, 056106 (2005).
[14] J. Rosa and M. W. Beims, Physica A **342**, 29 (2004).
[15] J. Rosa and M. W. Beims, Physica A **386**, 54 (2007).
[16] M. O. Scully and M. S. Zubairy, *Quantum Optics* (Cambridge University Press, Cambridge, 1997).
[17] J. M. Raimond, T. Meunier, P. Bertet, S. Gleyzes, P. Maioli, A. Auffeves, G. Nogues, M. Brune, and S. Haroche, J. Phys. B **38**, S535 (2005).
[18] P. Bertet, S. Osnaghi, P. Milman, A. Auffeves, P. Maioli, M. Brune, J. M. Raimond, and S. Haroche, Phys. Rev. Lett. **88**, 143601 (2002).
[19] A. Damjanović, I. Kosztin, U. Kleinekathofer, and K. Schulten, Phys. Rev. E **65**, 031919 (2002).
[20] H. Plohn, S. Krempl, M. Winterstetter, and W. Domcke, Chem. Phys. **200**, 11 (1995).
[21] M. Gruebele and P. G. Wolynes, Acc. Chem. Res. **37**, 261 (2004).
[22] I. Burghardt, M. Nest, and G. A. Worth, J. Chem. Phys. **119**, 5364 (2003).
[23] V. Bernshtein and I. Oref, J. Chem. Phys. **108**, 3543 (1998).
[24] Y.-C. Lai and C. Grebogi, Phys. Rev. E **54**, 4667 (1996).
[25] P. C. Rech, M. W. Beims, and J. A. C. Gallas, Phys. Rev. E **71**, 017202 (2005).
[26] U. Feudel, C. Grebogi, B. R. Hunt, and J. A. Yorke, Phys. Rev. E **54**, 71 (1996).
[27] L. Wang, G. Benenti, G. Casati, and B. Li, Phys. Rev. Lett. **99**, 244101 (2007).
[28] J. Rosa, C. Manchein, and M. W. Beims (unpublished).
[29] M. O. Magnasco, Phys. Rev. Lett. **71**, 1477 (1993).
[30] P. Reimann, Phys. Rep. **361**, 57 (2002).
[31] S. Kohler, J. Lehmann, and P. Hanggi, Phys. Rep. **406**, 379 (2005).
[32] R. D. Astumian and P. Hanggi, Phys. Today **55**, 33 (2002).
[33] J. B. Gong and P. Brumer, Annu. Rev. Phys. Chem. **56**, 1 (2005).
[34] C. Blomberg, Phys. Life. Rev. **3**, 133 (2006).
[35] W. Neupert and M. Brunner, Nat. Rev. Mol. Cell Biol. **3**, 555 (2002).
[36] J. L. Mateos, Phys. Rev. Lett. **84**, 258 (2000).
[37] W. H. Press, S. A. Teukolsky, W. Vetterling, and B. Flannery, *Numerical Recipes in Fortran* (Cambridge University Press, Cambridge, 1992).
[38] J. D. Bao, Y. Abe, and Y. Z. Zhuo, Physica A **277**, 127 (2000).
[39] T. Sintes and K. Sumithra, Physica A **312**, 86 (2002).
[40] L. Machura, M. Kostur, P. Talkner, J. Luczka, F. Marchesoni, and P. Hänggi, Phys. Rev. E **70**, 061105 (2004).